SCALING UP THE PROPULSION SYSTEM OF AN AERIAL AND SUBMERSIBLE MULTIROTOR VEHICLE

By

MICHAEL STEFAN CZERHONIAK

A thesis submitted to the

School of Graduate Studies

Rutgers, The State University of New Jersey

In partial fulfillment of the requirements

For the degree of

Master of Science

Graduate Program in Mechanical and Aerospace Engineering

Written under the direction of

Francisco Javier Diez-Garias

And approved by

_____

_____

_____

New Brunswick, New Jersey

January 2018

ABSTRACT OF THE THESIS

Scaling Up the Propulsion System of an Aerial and Submersible Multirotor Vehicle

By MICHAEL STEFAN CZERHONIAK

Thesis Director:

Francisco Javier Diez-Garias

A multirotor vehicle capable of operating in air and underwater developed at Rutgers has opened the door for combined aerial and underwater operations. The current vehicle is unable to carry out payload based missions due to low thrust outputs. This study examines the effects of scaling motors and propellers to larger sizes in air and underwater. Motor tests were conducted on two of the largest commercially available motors measuring rotational speed, current input, and torque load. These two motors were then compared with each other and smaller scale motors with regards to the torque load, power output, and efficiency. Afterward, three varying size motor-propeller combinations were examined in air and underwater. For each of these tests, the rotational speed, current input, torque output and thrust output were measured. Torque and thrust were observed to hold a linear relation with each other regardless if the system was in air or underwater. Performance for motor-propeller combinations were observed to increase along with size in air, but was more varied underwater.

Table of Contents

Abstract ii
Table of Contents iii
List of Tables iv
List of Equations iv
List of Figures v
1. Introduction 1
1.1. Literature Review 3
1.2. Theory 5
1.3. Thesis Overview 8
2. Experimental Set up 9
2.1. DAQ 9
2.2. Motor Setup 10
2.3. Propeller Setup 13
3. Results and Discussions 17
3.1. Motor Tests 17
3.2. Motor and Propeller Tests 20
3.2.1. Calculating Throttle 20
3.2.2. Torque-Thrust 21
3.2.3. Performance 26
4. Conclusion 35
4.1. Future Experiments 36
5. References 38

List of Tables

Table 1. Summary of motors and propellers 16

List of Equations

Mechanical Power Output 7
Electrical Power Input 7
Motor Efficiency 7
Performance 8

List of Figures

Figure 1. Breguet-Richet's Gyroplane No.1. 1
Figure 2. Amazon Prime Air and Domino's Pizza drones. 2
Figure 3. The Naviator, a multirotor aerial-underwater vehicle. 3
Figure 4. Micro-aerial vehicle 4
Figure 5. The stator and rotor of a brushless DC motor. 6
Figure 6. Torque/Speed characteristic of a brushless DC motor 7
Figure 7. Flow Diagram of a rotor. 8
Figure 8. Diagram for the DAQ board. 9
Figure 9. Image of the motor test setup 11
Figure 10. Diagram of the motor test setup. 12
Figure 11. Ideal Brushless DC motor curve. 13
Figure 12. Image of the motor and propeller test setup 15
Figure 13. Diagram of motor and propeller setup. 16
Figure 14. Motor speed and current consumption under a torque load for the large motors. 17
Figure 15. Power output under a torque load for the large motors. 18
Figure 16. Motor efficiency under a torque load for the large motors 19
Figure 17. Motor power output and efficiency comparison. 20
Figure 18. Calculating the PWM signal for zero RPM. 21
Figure 19. Torque-thrust relation for the Gemfan 5 by 3 inch carbon fiber propeller. 22
Figure 20. Torque-thrust relation for the T-motor 13 by 4.4 inch carbon fiber propeller. 23
Figure 21. Torque-thrust relation for the T-motor 28 by 9.2 inch carbon fiber propeller. 24
Figure 22. Comparison of the torque-thrust relations in air 25
Figure 23. Comparison of the torque-thrust relations underwater. 26
Figure 24. Performance of the Gemfan 5 by 3 inch carbon fiber propeller. 27
Figure 25. Performance of the T-motor 13 by 4.4 inch carbon fiber propeller. 28
Figure 26. Performance of the T-motor 28 by 9.2 inch carbon fiber propeller. 29
Figure 27. Comparison of the performances of the three motor-propeller combinations in air. 30
Figure 28. Comparison of the performances of the three motor-propeller combinations underwater. 31
Figure 29. Power and efficiency curves for the T-motor MN4006-23 motor. 32
Figure 30. Maximum torque comparison for the medium motor-propeller combination 33
Figure 31. Power input comparison for the medium and large sized motor-propeller combination in air. 34
Figure 32. Power input comparison for the medium and large sized motor-propeller combination underwater. 35

1. Introduction

The history of multirotor vehicles has its origins begin in the early 1900s with the Breguet-Richet Gyroplane No. 1, shown in Figure 1. This vehicle weighed 578 kg and was powered with a 36.7 kW engine. However, due to the technical limits of the era, control of the aircraft could not be achieved. There has been a resurgence of interest in the field with the introduction of brushless motors and other technologies.[1] Such technologies allowed the development of unmanned aerial vehicles (UAVs). UAVs have been especially useful due to their ability to hover. This ability allows for surveillance or inspection of disaster sites or for building inspections, as well as for recreational and civilian use.[2] In addition, UAVs show potential in military applications, weather research, and agriculture applications to name a few more specific examples.[3]

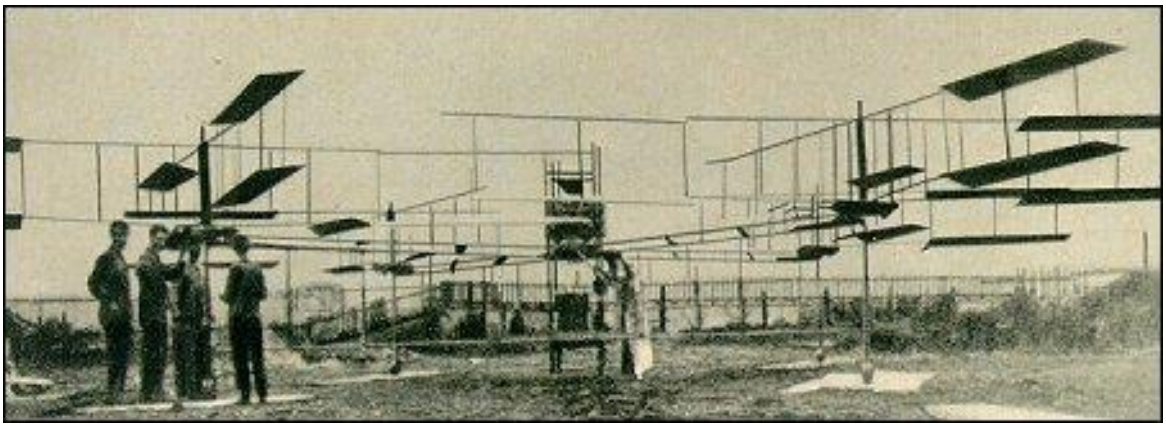

Figure 1. Breguet-Richet's Gyroplane No.1: One of the first multirotor vehicles (1907).

There exists a bright future for this technology as companies are investing in its future. One innovation in this rising technological field is a miniature UAV drone capable of delivering goods. Amazon plans to utilize such technology as part of their Amazon Prime Air program. The

goal of this program would be use GPS to autonomously fly packages to their destination within 30 minutes. Even food companies (Domino's Pizza as one example) plan to utilize a similar concept for food delivery.[4] Figure 2 shows both of these examples as concepts.

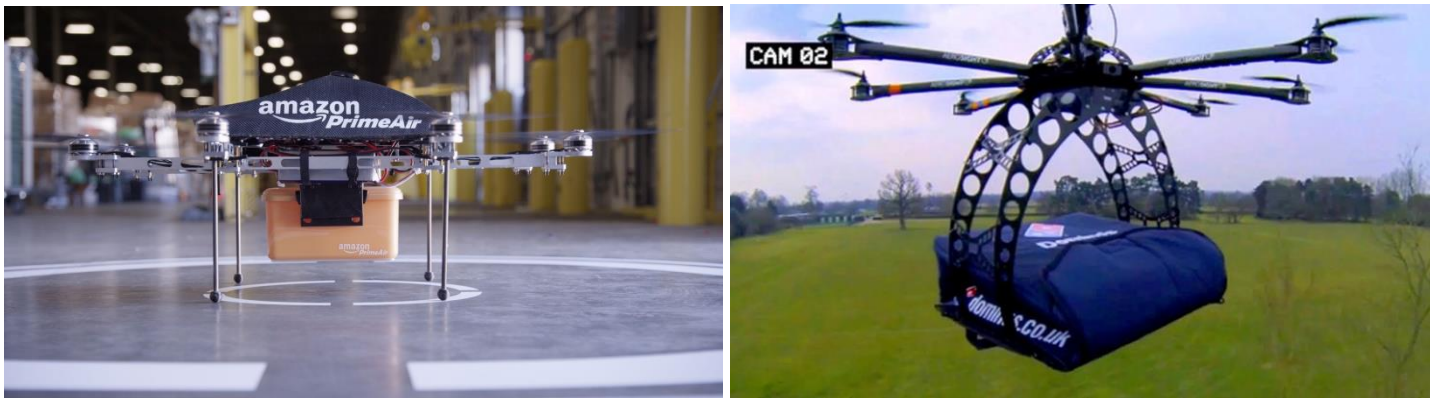

Figure 2. Amazon Prime Air (left) and Domino's Pizza (right) drones.

Aerial applications are not the only option for multirotor vehicles. Studies at Rutgers University have produced the first fully functioning vehicle that not only operates in air and underwater, but is also capable of seamlessly transitioning between the two medium. A vehicle capable of such feats further expands the possibilities of UAVs. With the addition to the uses in air, this type of vehicle will be able to survey underwater for pollution and erosion, as well as be able to perform inspections on structures like ships, bridges, and oil platforms to name a few examples. Figure 3 features the current model for the multi-medium vehicle.[5]

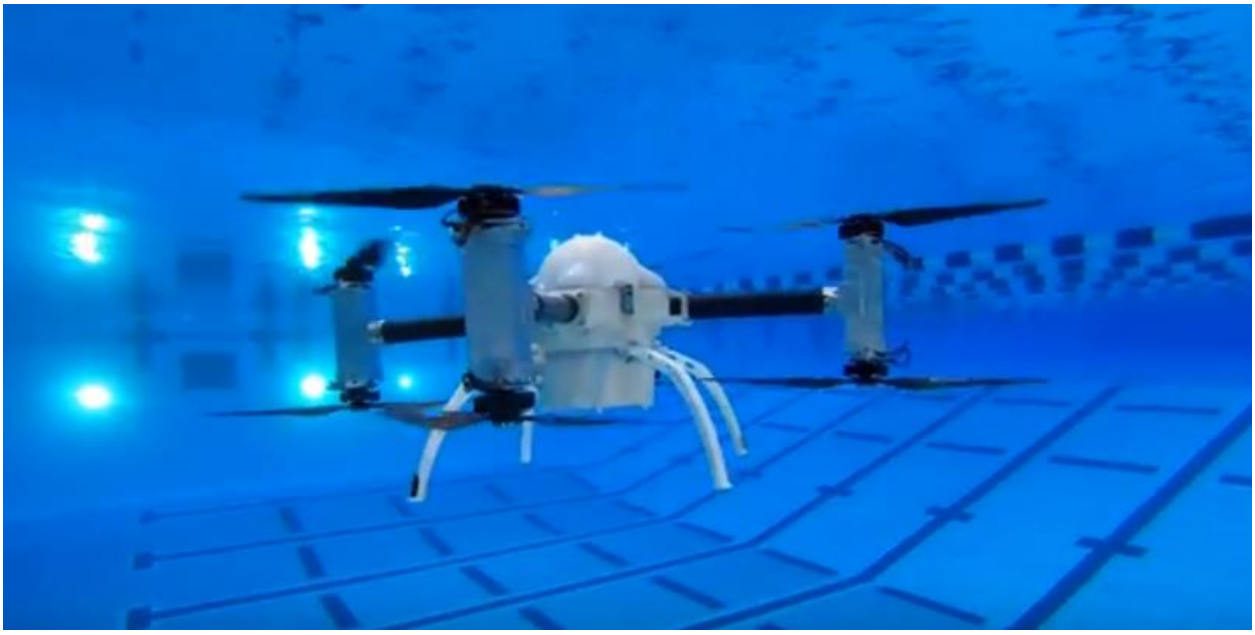

Figure 3. The Naviator, a multirotor aerial-underwater vehicle.

1.1. Literature Review

All motors considered for this study will be brushless DC motors. These motors are viewed by many as the more efficient option for a propulsion system for a multi-rotor vehicle. A team at Georgia Institute of Technology used these motors for their research in a method for design of a UAV electric drive system.[6]

A second type of electric motor for multi-rotor vehicles is the brushed motor. However, Winslow et al[7] found these motors to be more efficient on micro-aerial vehicles (MAV). These types of multirotor vehicles tend to have a gross weight of less than 50 g. As this study concerned increasing the size of the propulsion system, brushed motors were not considered for this study. A size comparison of a MAV can be seen in Figure 4.

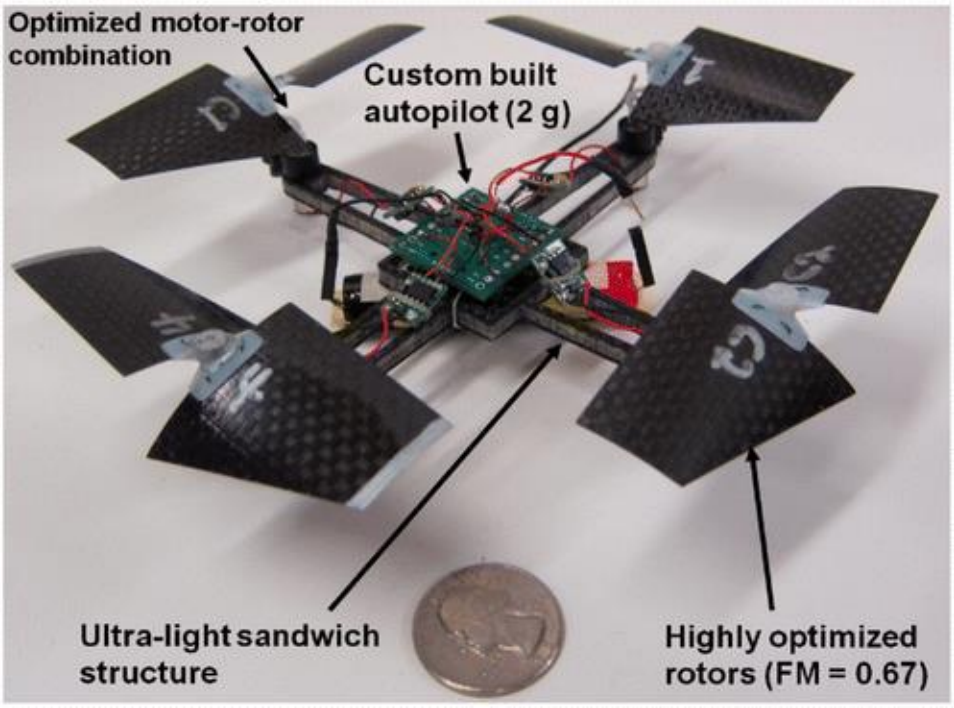

Figure 4. Micro-aerial vehicle.[7]

In addition to motors, propellers will be examined as the second focus of propulsion for this study. With a need for propeller data, Merchant[8] conducted tests on over 30 different propellers ranging in material (wood, glass fiber and carbon fiber) and diameter (from 6 to 22 inches). Further data on propellers was collected with Brandt and Selig.[9] Together they tested 79 propellers within the diameter range of 9 to 11 inches. During their tests, it was observed among these propellers that the most efficient was calculated to be 65%, while the least efficient was 28%.

The effect of separation distance of propellers on a quadcopter was examined by Yoon et al.[10] Their found that as the gap between rotors decreased, so did the efficiency of the quadcopter system. A similar result was found by Intaratep et al.[11] Despite being an acoustic study, thrust data was also taken. In their study, when two rotors were in use, thrust was reduced by 5.8%,

while when four rotors were used the thrust was reduced by 7.3% in comparison to a scaled single rotor.

Gap size between rotors was further examined by Aleksandrov and Penkov.[12] An 8 inch and 10 inch propeller, both with 4.5 inch pitch were used for their tests. Thrust was found to increase as the gap widened form 5 mm to 35 mm. The optimal distance for the rotors used in this study was found to be 32.65 mm.

Further experimentation on quadcopters has provided new ways of control. Ryll[13] et al have produced a prototype quadcopter which is capable of overcoming the mobility limitation on most quadcopters (4 control inputs vs. 6 degrees of freedom in space). They implemented a design that allowed for the rotors to be able to be rotated. This makes it possible for full control for the 6 degrees of freedom.

Unlike research for UAVs, information for multi-medium vehicles is scarce. Research done by Soni[14] provided an approach for modelling motors and propellers in air and water. The results of his research were incorporated into the design of the multi-medium vehicle, the Naviator. Maia et al[5] have developed this vehicle to perform in both air and water, as well as seamlessly transition between the two medium.

1.2. Theory

A brushless DC motor is a type of synchronous motor, where the magnetic field produced by the stator rotates with the same frequency of the magnetic field generated by the rotor. The stator is the non-rotating part of the motor which houses electromagnetic coils wrapped around a layered steel core. The rotor is the rotating portion of the motor which consists of permanent

magnets of alternating North and South poles.[15] Figure 5 displays a brushless motor's stator and rotor.

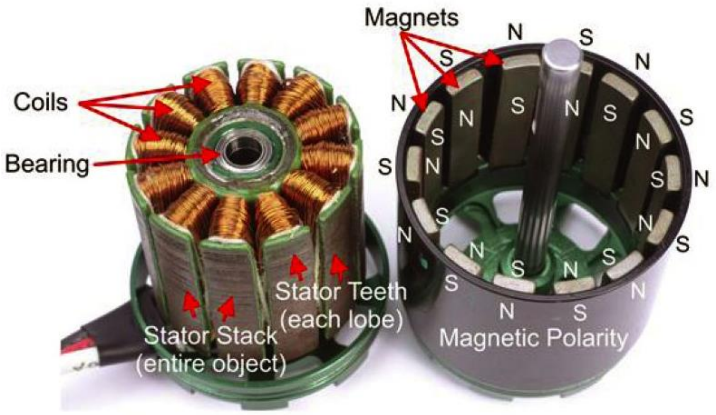

Figure 5. The stator (left) and rotor (right) of a brushless DC motor.

Communication of a brushless DC motor is done electronically. In order to rotate the motor, the stator windings are energized in sequence. The position of the rotor dictates which stator will be energized. Rotor position is tracked with the use of back Electromotive Force (back EMF) sensors. Back EMF is a voltage generated by the stator windings, as a result of the motor's rotation, which opposes the main voltage supplied to the windings. Back EMF sensing methods are suitable for high and low voltages, as well as high and low speed applications.[16]

A characteristic of brushless DC motors is the linear relation between the motor speed and torque load.[15] With no load, the maximum speed of the motor is achieved, but as a torque load is introduced, the speed of the motor decreases, as shown in Figure 6. A similar characteristic is observed between current and torque. However, current consumption will increase as a torque load is increased.[17]

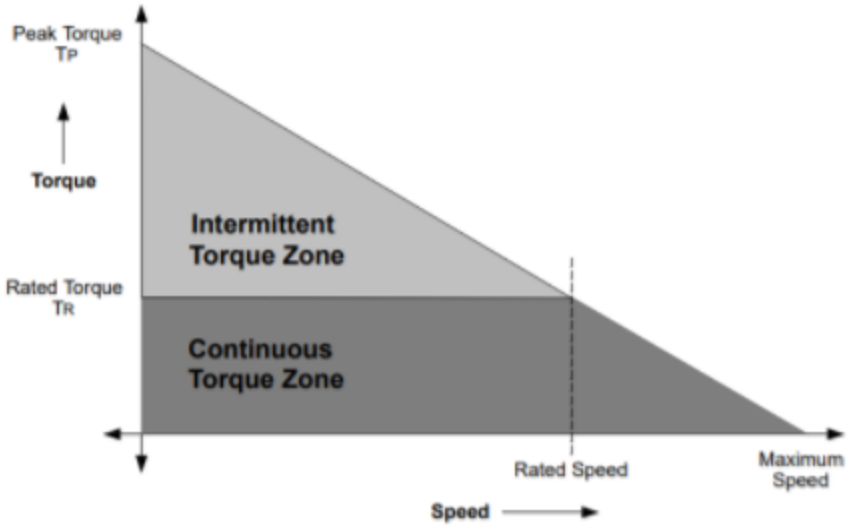

Figure 6. Torque/Speed characteristic of a brushless DC motor.[15]

Mechanical power output (P_{out}) for a motor can then be calculated from the motor speed (ω, in radians pes second) and the torque load (Q). Electrical power input (P_{in}) for the motor can be obtained with the input voltage (V) and the current consumed by the motor (i). The two powers can be then used to determine the efficiency of the motor (η).

$$\textbf{Mechanical Power Output: } P_{out} = \omega * Q \quad \{1\}$$

$$\textbf{Electrical Power Input: } P_{in} = i * V \quad \{2\}$$

$$\textbf{Motor Efficiency: } \eta = P_{out} / P_{in} \quad \{3\}$$

In addition to motors, this study also looks at propellers for a propulsion system. The mechanical power produced by the motor accelerates the air in the disk area of the rotating propeller. Thrust (T) is generated as a result of the accelerated air.[18] This is demonstrated in Figure 7.

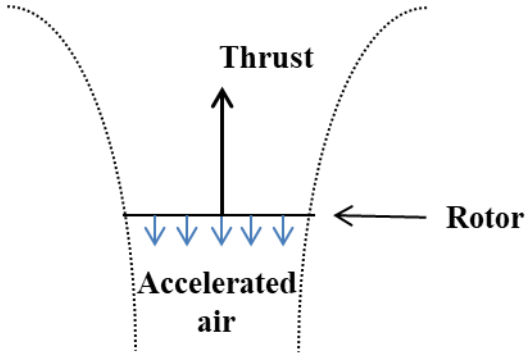

Figure 7. Flow Diagram of a rotor.

An effective way to establish a motor-propeller combination's potential would be to communicate a how well the combination can produce thrust per the electrical power input. Rather than looking at the efficiency of a combination, the performance (Π) will be examine in this study.

$$\textbf{Performance: } \Pi = T / P_{in} \qquad \{4\}$$

1.3. Thesis Overview

This study is meant to further enhance the capabilities of this multi-medium vehicle. The current testing vehicle is yet capable of carrying any payloads. One solution the problem presented is to increase the thrust output. The objective of this study is to observe the effects on increasing the propulsion system of a multi-medium vehicle. Propulsion system involves motors, propellers, ESC and batteries. This study will focus on the first two.

Section 2 of this thesis will explain the experimental setups used for this study, as well as the method for data collection. Section 3 will examine the results of the experiments conducted during this study. Section 4 will discuss the conclusions from the previous section, and consider options for future studies.

2. Experimental Set up

2.1. DAQ

Data for all experiments was collected using a Data Acquisition Unit (DAQ) system. As shown in Figure 8, the device is equipped with an Arduino, two HX711 load cell amplifiers, two ACS712 current sensors, several ports for various sensors, a screen, and a micro SD port. It is powered by a 2 cell LIPO battery (7.4 V).

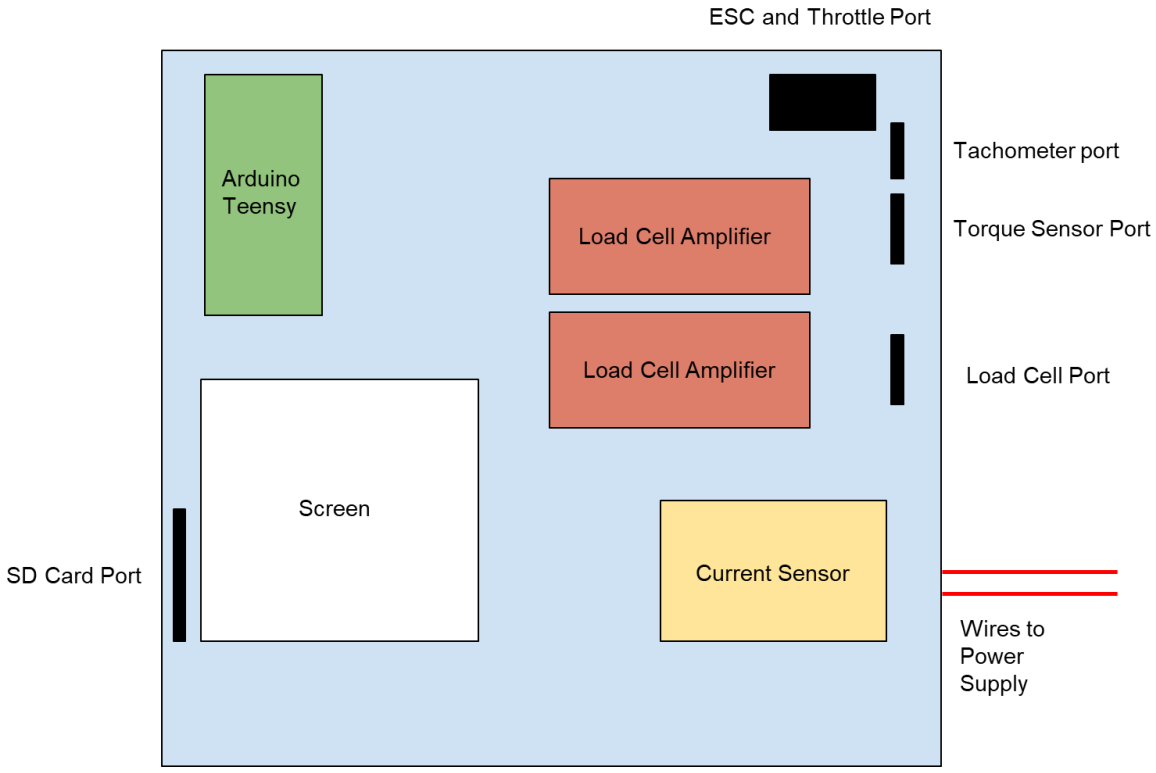

Figure 8. Diagram for the DAQ board. Not included in this diagram are serval buttons which are used to start and pause data collection and to open new files.

The HX711 load cell amplifiers are used to detect the resistance in a corresponding load cell. The Arduino can then read and scale the measurement to the proper force. Each load cell

amplifier is connected to one of the load cell ports. For the experiments conducted, one port was designated for a torque load cell, while the other was for a force load cell.

Similar to the load cell amplifier, the ACS712 current sensors were used to collect raw data to be sent to the Arduino. One of the sensors was used for smaller current loads (up to 5 A), while the other was used for larger currents (up to 30 A). Due to the demand of higher current for the experiments performed, the 30 A sensor was more predominantly used over the 5 A sensor.

Besides the current sensors, all other sensors were connected to the DAQ using the several ports on the board. The two load cell ports were connected to the load cell amplifiers, whereas all other ports were directly connected to the Arduino. A DT-2234C+ digital tachometer was used to collect data on the motor speed, in RPM. This device was rewired to be able to send its signal to the DAQ via the tachometer port. A servo tester, used for throttle control, was connected to the DAQ to send its signal to both the DAQ and an electronic speed controller (ESC), which communicates a pulse width modulation (PWM) signal to the motor. Both the servo tester and ESC are connected to the DAQ by the same port.

The screen displayed raw values for the data to be collected by the sensors. These values were used to monitor the experiment before and during the data collection process. All data collected by the DAQ is saved and stored onto a micro SD, which is then transferred to a computer for processing.

2.2. Motor Setup

In order to add payloads to future testing vehicles, larger thrusts need to be produced. One solution to produce more thrust is to use bigger propellers, and a result, larger motors will

be needed. For this purpose, two of the largest commercially available motors, the T-motor U8 Pro and the T-motor U10, were used.

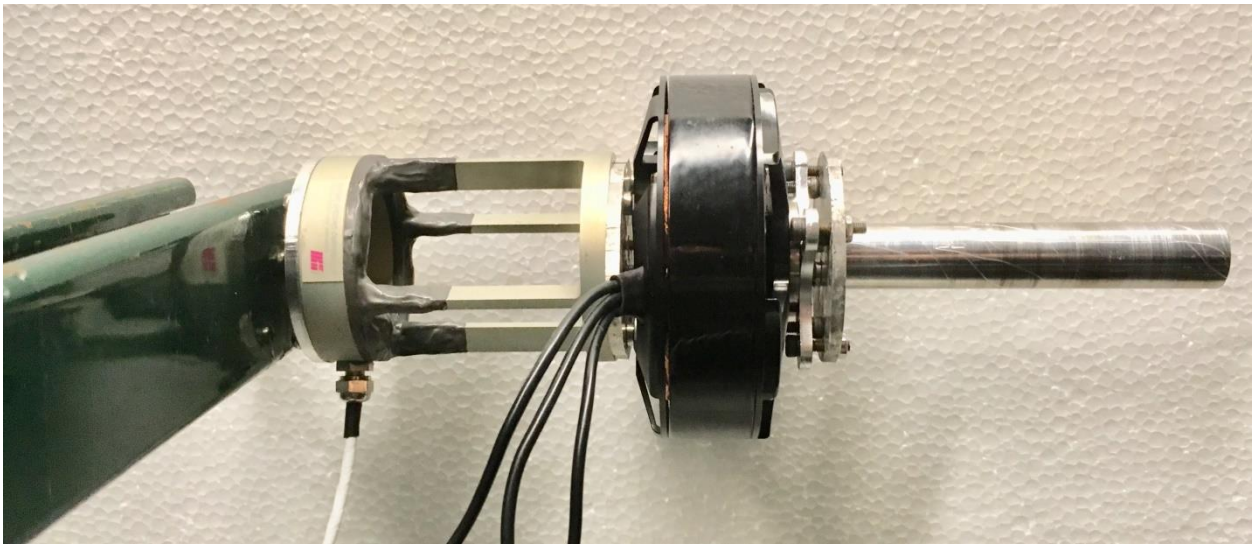

Figure 9. Image of the motor test setup with the T-motor U10 motor. The motor is equipped with a brake to introduce torque into the system, which is detected by the torque sensor attached to the other end of the motor.

The motor testing setup used three sensors to collect data: a Sensing Systems 1 N*m torque sensor, a DT-2234C+ digital tachometer, and the 30 A current sensor on the DAQ. Rather than a battery, the motor was powered by a Maisheng DC power supply. The voltage on the power supply was held at a constant 22.2 V, the nominal voltage of a 6 cell LiPo battery. To power the motor, the power supply was connected to the DAQ and the ESC. A servo tester was used as a manual throttle control for the motor. It sends its signal to the DAQ which then send it to the ESC and the motor.

The motor is mounted onto the torque sensor, which is mounted to a support beam secured to the lab table. The support beam was extended from the edge of the table and secured

with another support to prevent any vibrations. The torque sensor was connected to the DAQ via one of the load cell ports to communicate data. Similarly, the digital tachometer was connected to the DAQ via tachometer port. The device was secured in a way to ensure the laser would target the motor. The laser is then reflected off the motor via a piece of reflective tape and sent back to the tachometer and then is processed to give the motor speed. An aluminum brake arm is attached to the motor to provide a torque load. The load is applied by gripping the brake arm while the motor is running. A glove is worn for safety purposes.

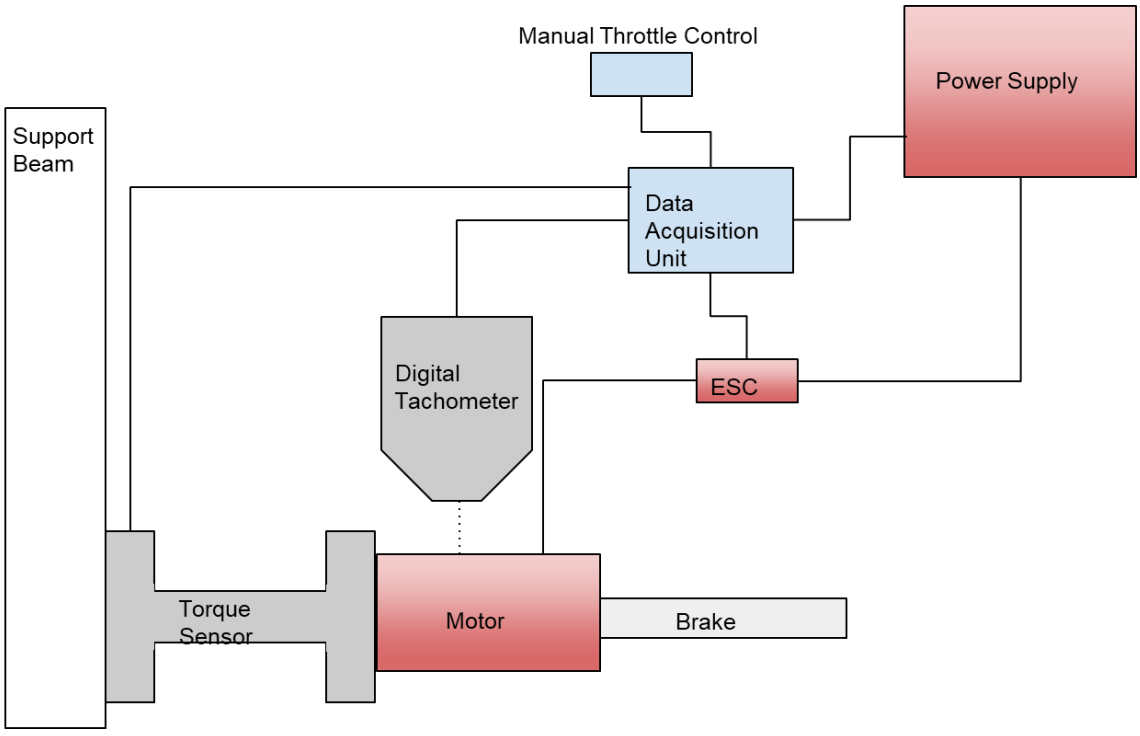

Figure 10. Diagram of the motor test setup.

Motors for this experiment were run at maximum throttle. Data for this experiment was limited by the torque sensor, as no torque load should exceed 1 N*m. The screen on the DAQ was used to monitor the torque applied so it does not exceed that value.

Data collected from this setup will be used to replicate the four plots displayed in Figure 11. Each of the plots is valued against increasing torque load. The motor speed and current consumption plots are the two linear lines on the plot. The declining line represents the motor speed (in RPM), while the inclining line represents the current consumption (in Amps). Power output generated (in Watts) is represented by the parabola, peaking at half the stall torque. The final curve represents the efficiency of the motor.

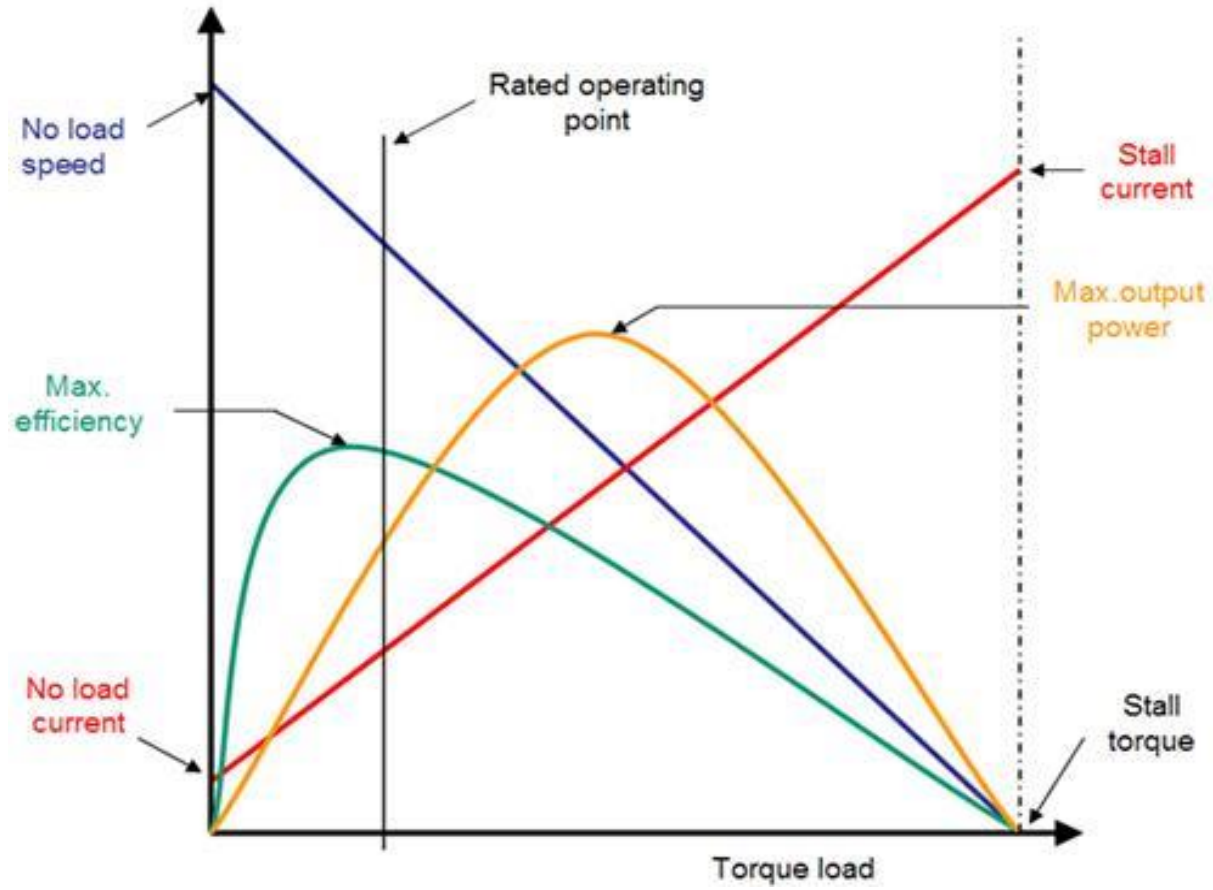

Figure 11. Ideal Brushless DC motor curve.

2.3. Propeller Setup

Propeller and motor testing is done with a similar setup as the motor tests. In addition to the sensors used for the motor test, a standard scale 10 kg load cell was used to measure thrust in

grams force. This sensor is secured to between the torque load cell and the support beam. Data collection for these tests included thrust, torque, motor speed and current consumed. Air tests were conducted in a similar way to the motor tests, while water tests were conducted either in a 126 gal water tank or the lab's water tunnel, depending on the size of the propeller.

Three different sized motors were used for the propeller test for varying sized propellers. The first was the NTM Propdrive 28-26 1000 kV motor. This motor was run with 14 V of power supplied from the Maisheng power supply. This motor was used for various sized small propellers ranging in diameter sizes from 3 in to 6 in. All the propellers tested on this motor were tested in the water tank for the water tests. This motor, along with the propeller it is equipped with, will be referred as a small motor-propeller combination.

The second motor was the T-motor MN4006-23 380 kV, which was run at 22.2 V from the power supply. This motor was equipped with a T-motor carbon fiber 13 inch diameter by 4.4 inch pitch. All motors of this type within the lab were repurposed from previous test vehicles. To account for this, several of these motors were tested using the same propeller and ESC for maximum thrust, motor speed, and current consumption. The most consistent of these motors were selected for experiments using these motors. Due to the size of the propeller, the water test for this motor combination was conducted in the water tunnel. This motor, along with the propeller it is equipped with (ranging from 10 inches to 15 inches), will be referred as a medium motor-propeller combination.

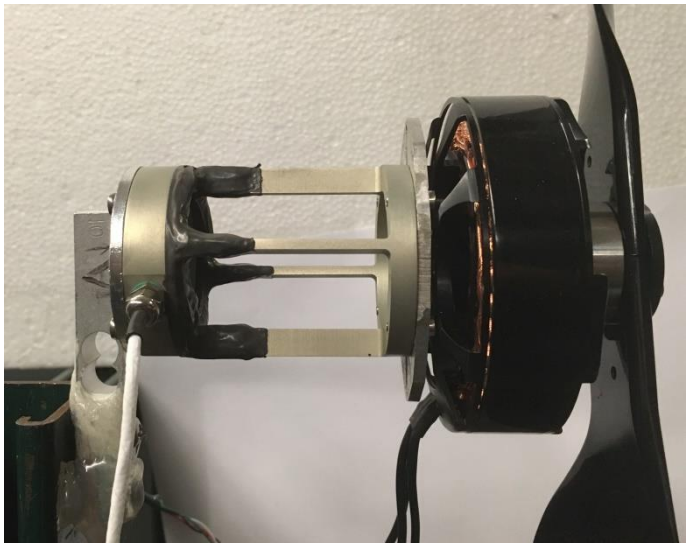

Figure 12. Image of the motor and propeller test setup with the T-motor U10 motor equipped with the T-motor 28 by 9.2 inch carbon fiber propeller. The propeller replaces the brake from the motor setup, and the torque sensor is now attached to a load cell.

The final motor used for testing the largest propellers was the T-motor U10 100 kV motor. Like the previous motor, this motor was run at 22.2 V. It was equipped with a T-motor carbon fiber 28 inch diameter by 9.2 inch pitch propeller (Figure 12). Like the previous motor and propeller combination, the water test for this combination is also performed in the water tunnel. This motor and propeller combination was required to be monitored, as the larger size of the propeller meant more torque will be produced. High torques were observed in both air and water tests. This motor, along with the propeller it is equipped with, will be referred as a large motor-propeller combination.

Motor Size	Motor	Motor Weight	Propeller	Input Voltage	Maximum Thrust	Maximum Torque	Maximum Power Input
Small	NTM Propdrive 28-26 1000 kV	54 g	Gemfan 5 by 3 inch	14.0 V	174.5 g	0.019 Nm	36.8 W
Medium	T-motor MN4006-23 380 kV	68 g	T-motor 13 by 4.4 inch	22.2 V	1154.5 g	0.109 Nm	199.5 W
Large	T-motor U10 100 kV	405 g	T-motor 28 by 9.2 inch	22.2 V	2395.9 g	0.778 Nm	203.9 W

Table 1. Summary of motors and propellers used, including the reference size, input voltage, and the maximum thrust, torque, and power input in air.

Table 1 displays a summary of the motors and propellers examined in this section. All water tests were unable to be run at maximum throttle due to the high currents being detected.

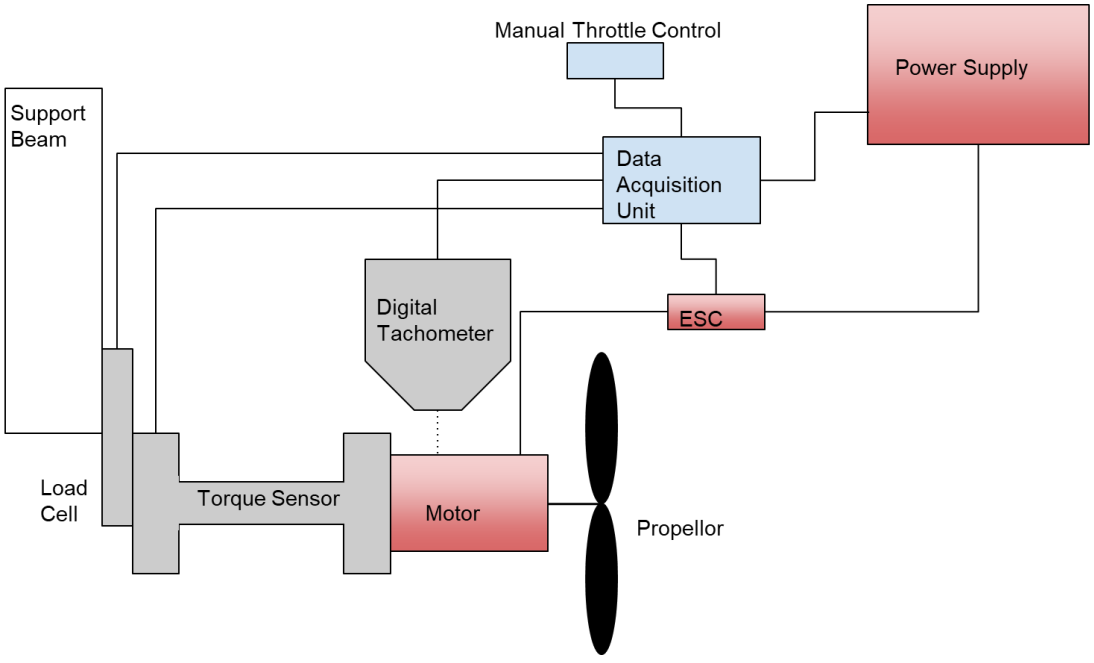

Figure 13. Diagram of motor and propeller setup.

3. Results and Discussions

3.1. Motor Tests

Torque, current, and motor speed data was collected for both the large motors selected, the T-motor U8 Pro and T-motor U10 motors. Due to limitations on the torque sensor, torques could not exceed 1 N*m for data collection. As such, motor stall could not be achieved via experimentation. However, like the ideal BLDC motor plot, it was observed that the sample of data taken for both the motor speed and current consumption held a linear relation with the torque load. A linear fit was performed on the collected data to estimate each motor's stall torque and stall current. The stall torque was obtained by extrapolating the motor speed vs torque data. The current vs torque data was then extrapolated to the stall torque to obtain the stall current for each motor. From Figure 14, it is observed that the stall torque, stall current, and no load speed for the U10 motor is greater than the U8 Pro motor.

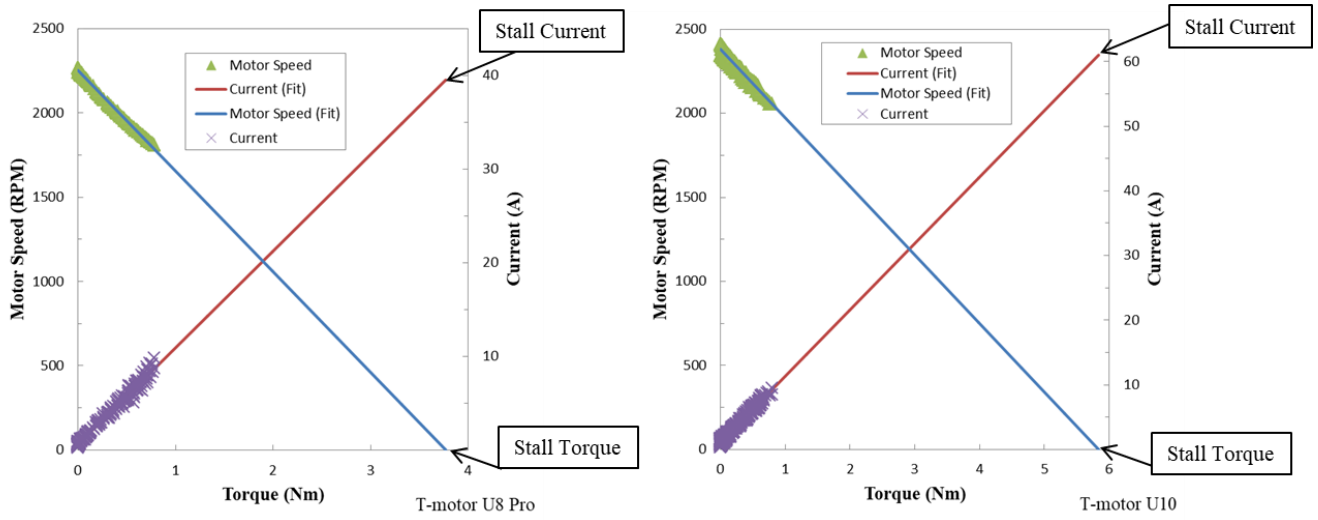

Figure 14. Motor speed and current consumption under a torque load for the T-motor U8 Pro and U10 motors. The U10 motor is observed to have a greater stall torque, stall current and no load speed than the U8 Pro motor.

Using the fitted motor speed data, the power output curve of both motors can be interpreted. Just like the ideal motor curve for power output, it is observed that the power output for both motors is a parabola, with its maximum at half the stall torque. Like the speed and current plots, it is observed in Figure 15 that the U10 motor has a higher power output.

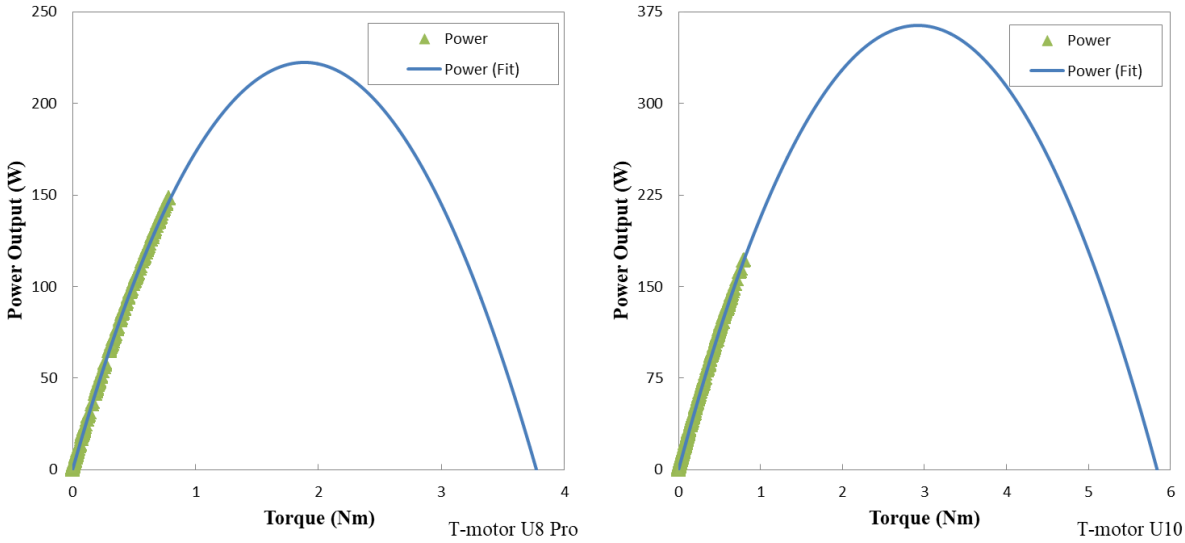

Figure 15. Power output under a torque load for the T-motor U8 Pro and U10 motors. The U10 is observed to have a greater maximum power output than the U8 Pro motor.

Likewise, the efficiency of both motors produced a curve similar to the ideal curve, peaking at a low torque, and then decreasing until the stall torque. From the power curve and the efficiency curve, a range maximum torques can be determined. Despite both motors peaking at 80% efficiency, the U10 motor maintains higher efficiencies as larger torque loads are applied as shown in Figure 16. Because a motor is less efficient as more torque is introduced, a motor and propeller combination should remain on the left half of a motor curve. Comparing the two large motors, it is evident that the U10 motor is superior to the U8 Pro motor. Especially when

considering use for underwater, the larger stall torque of the U10 motor is more desirable. For this reason, the U10 motor will be used for the largest propeller in the next section.

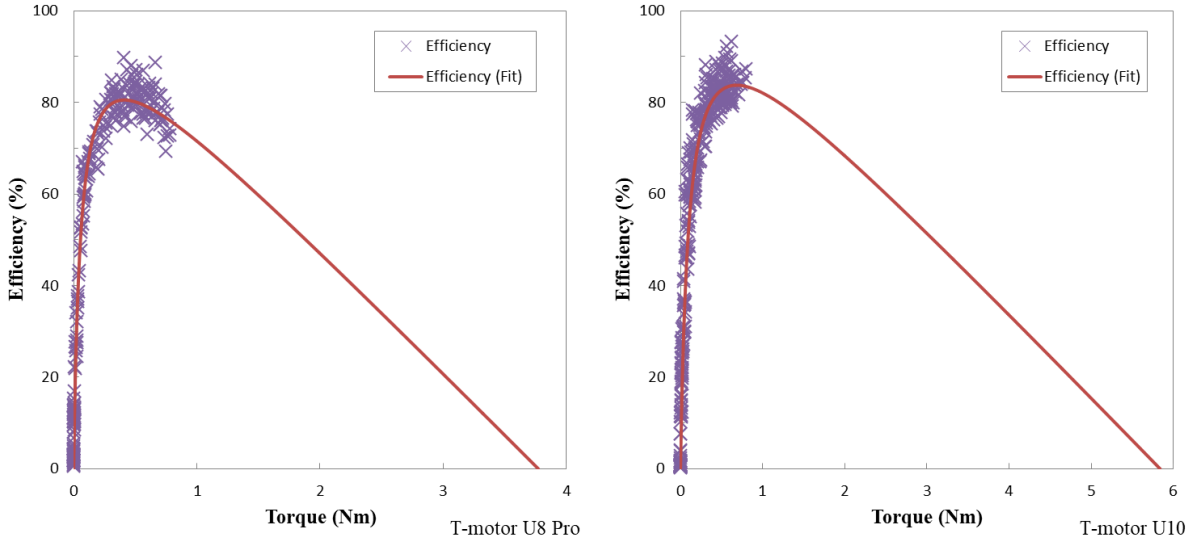

Figure 16. Motor efficiency under a torque load for the T-motor U8 Pro and U10 motors. Both motors are observed to reach 80% efficiency.

When comparing the power output, stall torque, and efficiencies of both the selected large motors to a much smaller motors, the effects of scaling are more evident. In addition to the two large motors being examined, Figure 17 shows two different motor sizes that will be examined with propellers. The smallest motor used was the NTM Propdrive 28-26 1000 kV motor operating at 12 V and at 16 V, while the other motor is the T-motor MN 4006-23 360 kV motor operating at 22.2 V. The difference in voltage of the smallest motor significantly influences its maximum power output. Despite the increase in power generated, the small motor still produces less power than the two large motors. Regardless of the voltage input, both the efficiency and stall torque of the small motor are vastly inferior to the large motors. Likewise the

second motor is observed to have a smaller maximum power output and stall torque than the large motors. Scaling from the smallest motor to the second motor does little to change these parameters as well. However, the second motor's big advantage to scaling up from the NTM motor is that it is much more efficient, even more so that the larger two motors.

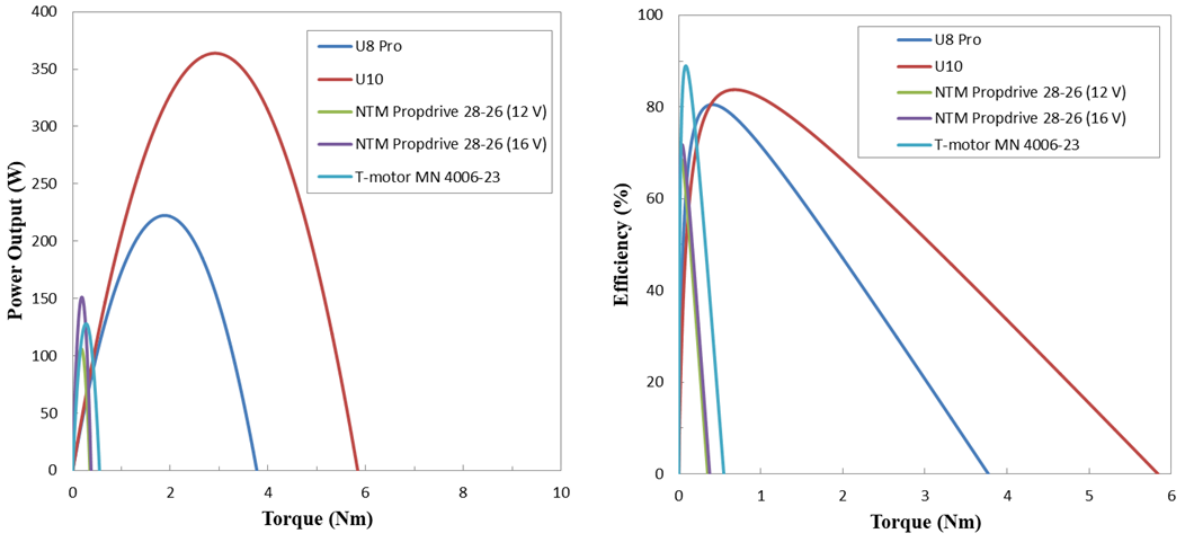

Figure 17. Motor power output and efficiency comparison.

3.2. Motor and Propeller Tests

3.2.1. Calculating Throttle

Each motor is operated with a manual throttle control which sends a PWM signal to the ESC. Once a certain PWM signal threshold is met for the ESC, it communicates to the motor to begin operating. However, as Figure 18 shows, the motor's speed is not 0 when the motor begins to operate. A polynomial fit was used to determine at what PWM signal value the motor would produce 0 RPM. This PWM value was set as the 0% throttle for the motor, whereas the PWM value corresponding to the maximum RPM would be considered 100% throttle for the motor. Changing motors or ESCs was found to change the PWM value corresponding to 0% throttle.

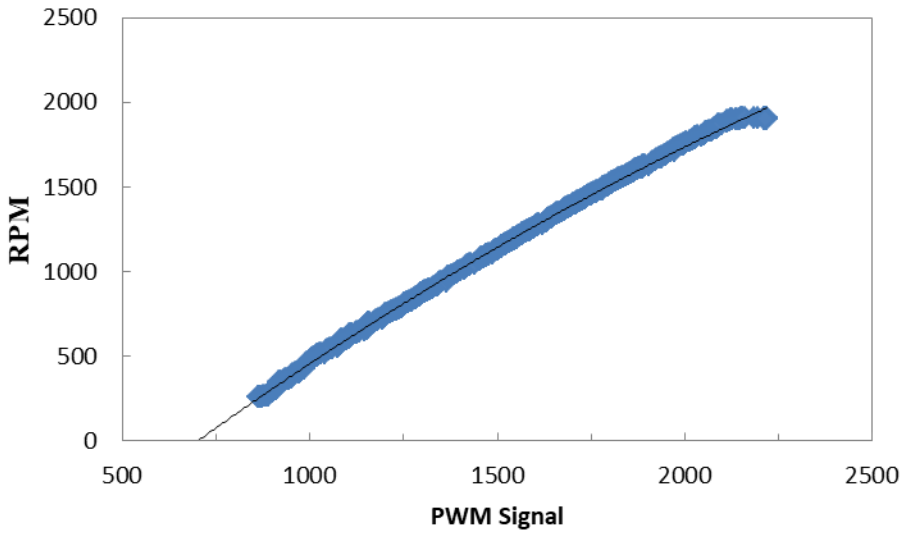

Figure 18. Calculating the PWM signal for zero RPM for the T-motor U10 motor with the 28 inch propeller. A second order fit was extrapolated to obtain the value for "0% throttle".

3.2.2. Torque-Thrust

A NTM PropDrive 28-26 1000 KV motor was equipped with several small propellers ranging in diameter size from 3 inches to 6 inches. All tests conducted on this motor and its propellers, both in air and underwater, were done with a 14 V input from the power supply. Despite each motor-propeller combination working in both air and water, a vast majority of propellers were disregarded from data collection due to the material of the propellers. All but the carbon fiber propeller experienced some form of deformation underwater, and as such only the Gemfan 5 inch diameter by 3 inch pitch carbon fiber propeller was used for the small motor-propeller combination.

In air tests it was observed that each motor-propeller combination had a unique linear torque thrust ratio. This trend was also observed when processing water experiment data, as

shown in Figure 19. Water introduces more torque to the system, and as a result more thrust is produced. This results in the linearity observed in air to continue underwater with a coefficient of variation of 2.28% for both air and water trials. Underwater testing was concluded due to high currents reaching the motor's limit.

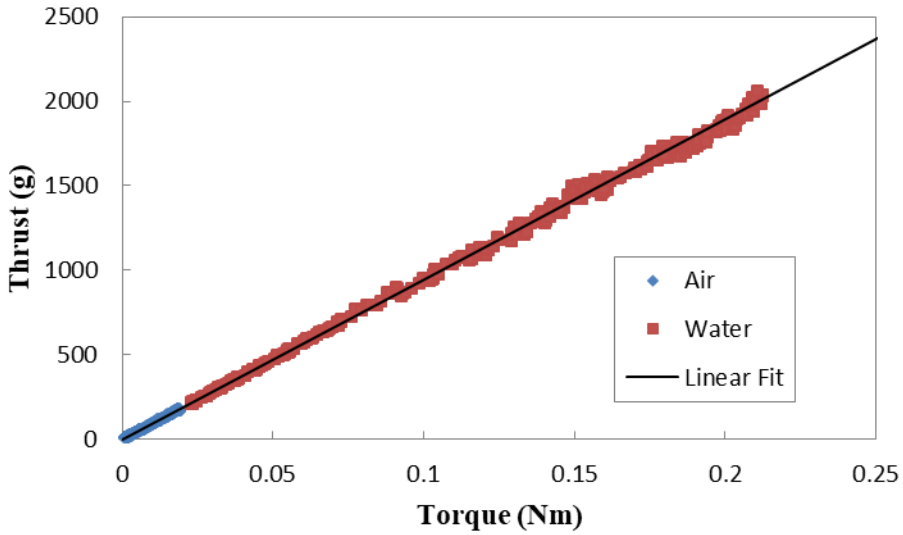

Figure 19. Torque-thrust relation for the Gemfan 5 by 3 inch carbon fiber propeller in air and water. Underwater data was concluded at 60% throttle due to high current consumption.

Air and water experiments continued by scaling up to the T-motor MN4006-23 380KV motor and T-motor 13inch diameter by 4.4 inch pitch. The voltage in the power supply was increased to 22.2 V from the 14 V used to power the smaller motor. This voltage was selected as it is the nominal voltage of a six cell LiPo battery, the size batteries used to power the same motor and propeller on the Naviator.

Like with the smaller motor combination, a linear relation between torque and thrust was observed (Figure 20). Including the manufacture data (provided online), the coefficient of

variance for the air and water trials was 2.97%. The manufacture data for the motor and propeller combination had an input voltage of 24 V from a non-specified DC power supplier. Despite this increase in voltage, no significant change is observed in the relation of torque and thrust produced by the motor and propeller combination. As with the small motor-propeller combination, water testing for this motor-propeller combination was concluded due to high currents being recorded, approaching the limit on the current sensor.

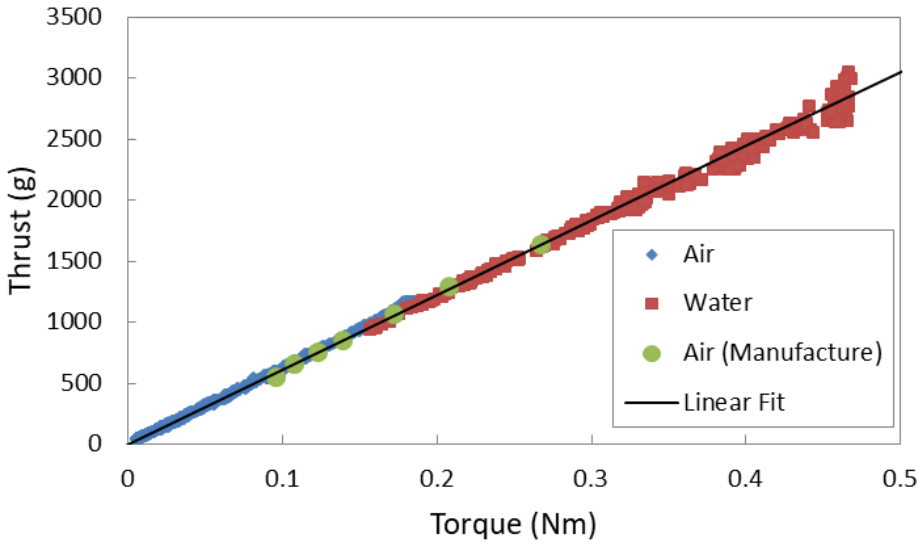

Figure 20. Torque-thrust relation for the T-motor 13 by 4.4 inch carbon fiber propeller in air and water. The manufacture data was obtained online; it was run with 24 V power supply. Underwater data was concluded at 40% throttle due to high current consumption.

The next experiments were done with the T-motor U10 motor and T-motor 28 inch diameter by 9.2 inch pitch. For consistency with the medium combination, the power supply remained at 22.2 V. With the vast increase in size of the propeller, much more torque was expected of being produced, and as such, unlike the smaller combination, the air trials had to be

monitored so as to not exceed the 1 N*m limit on the torque sensor. Fortunately, air trials were able to reach max throttle without hitting the limit; max torque was observed to be 0.90 N*m.

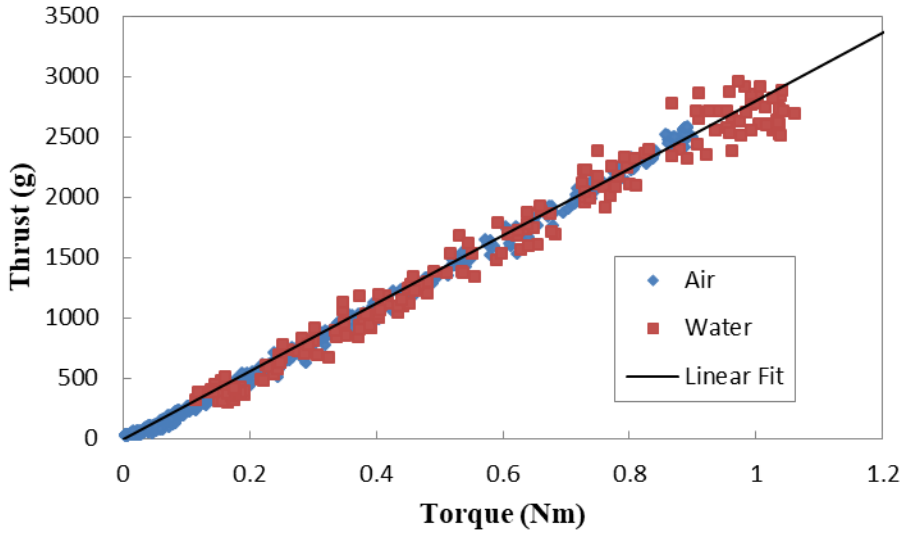

Figure 21. Torque-thrust relation for the T-motor 28 by 9.2 inch carbon fiber propeller in air and water. Underwater data was concluded due to torque sensor limits.

Likewise, monitoring of the system needed to be done for water tests. Unlike the previous two combinations discussed, the torque underwater reached the 1 N*m limit on the sensor. This was done at 17.5% throttle. Despite the data collection being stopped at low throttles, the torque-thrust relation in air and water is observed to be linear for larger propellers with a coefficient of variance of 6.42%. The higher variation can be attributed to the larger torque and thrust produced, which may have caused vibrations in the setup structure.

From Figure 22, it is observed that as the size of the propeller and motor increases, the torque-thrust ratio decreases. This is a result of more air (water) being required to be moved by an increasing propeller diameter. As a result, the smaller combinations can be observed to produce more thrust at lower torque loads. However, these combinations have a limit to thrust

output, and result in producing less thrust at higher throttles. At max throttle, the smallest combination produces less than 250 g of thrust compared to the 2500 g of thrust produced by the largest combination.

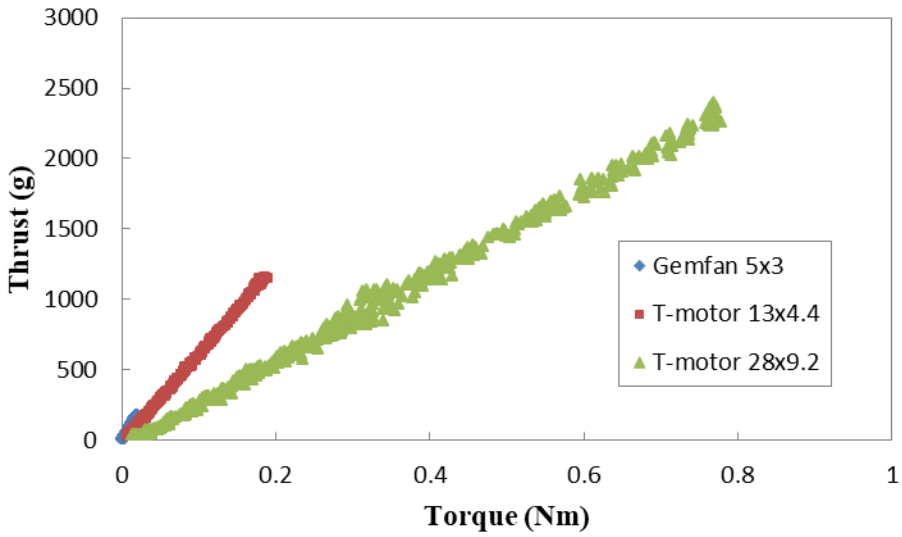

Figure 22. Comparison of the torque-thrust relations in air.

Likewise, underwater, the torque-thrust ratios decrease with increasing propeller size. As shown with the individual cases, the amount of thrust produced underwater is much greater than the amount produced in air. The underwater data taken for the 28 inch propeller was retaken without the torque sensor to observe thrust output at higher throttles. The torque was then estimated using the ratio found in Figure 21. As seen in Figure 23, the 28 inch propeller is expected to produce torques greater than 3.5 Nm at higher throttles.

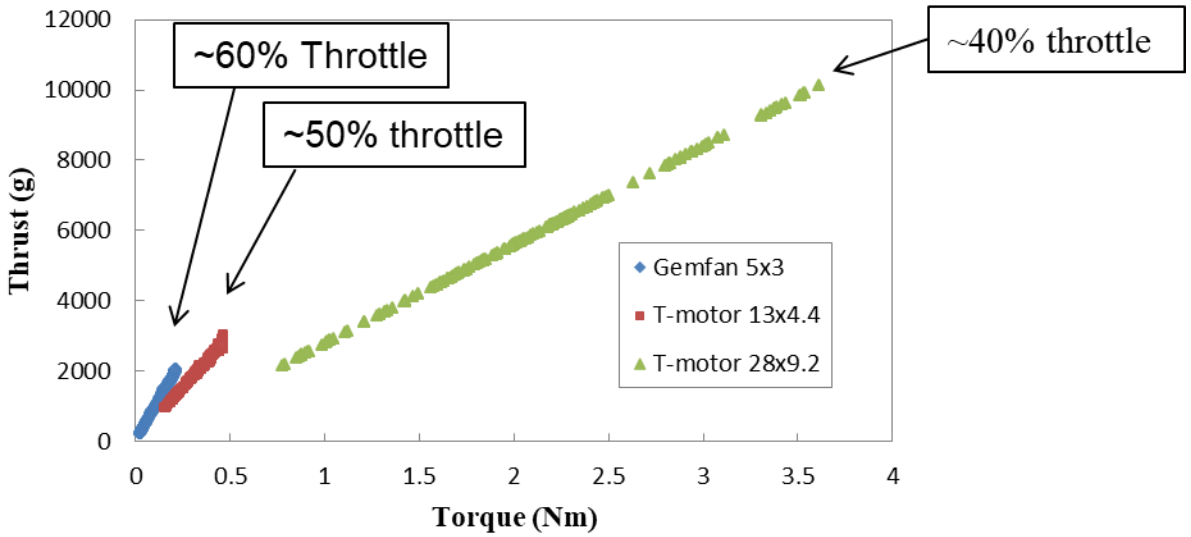

Figure 23. Comparison of the torque-thrust relations underwater. Torque for the 28 inch propeller was estimated by using its torque-thrust ratio.

3.2.3. Performance

Further analysis was done towards examining the performance of the motor-propeller combination in air and water. Unlike in the motor tests where efficiency (power output per power input) is more steadily looked at, motor-propeller combinations look at the performance, or more accurately the thrust output per power input. Similar to the torque-thrust examination, the performance for each motor propeller combination will first focus on each individual combination, before comparing the air and water cases.

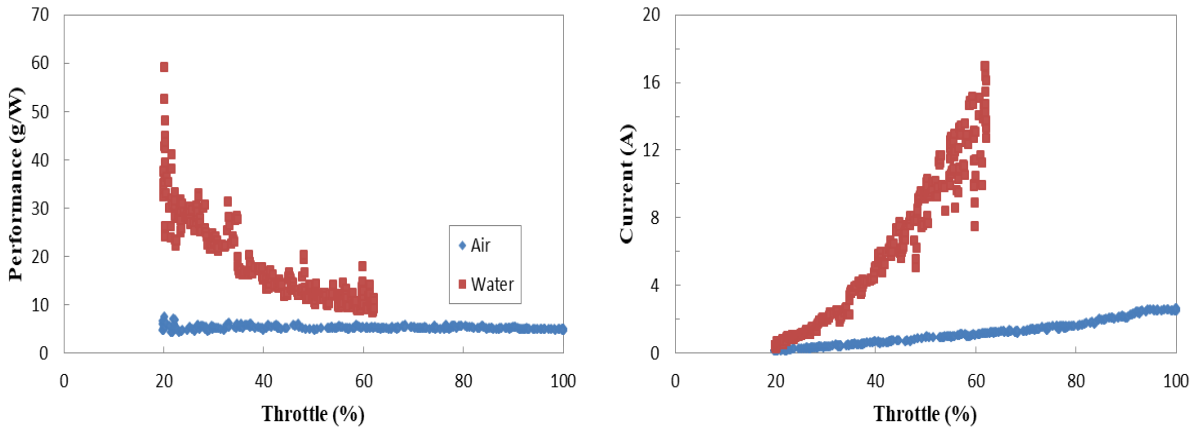

Figure 24. Performance of the Gemfan 5 by 3 inch carbon fiber propeller in air and water. Underwater data was concluded at 40% throttle due to high current consumption.

Immediately looking at the data presented in Figure 24 for the NTM motor with the Gemfan 5 inch propeller, it is observed that underwater performance is much greater than performance in air. The air performance for this combination stays relatively consistent throughout the throttle range, whereas the underwater performance gradually decreased with increasing throttle. More force is needed to push water than air, thus more thrust is produced underwater; however, more power is then required to operate the motor and propeller underwater. As a result, more current was consumed by the motor-propeller combination underwater than in air. Underwater tests were concluded before reaching 100 percent throttle due to high current consumption.

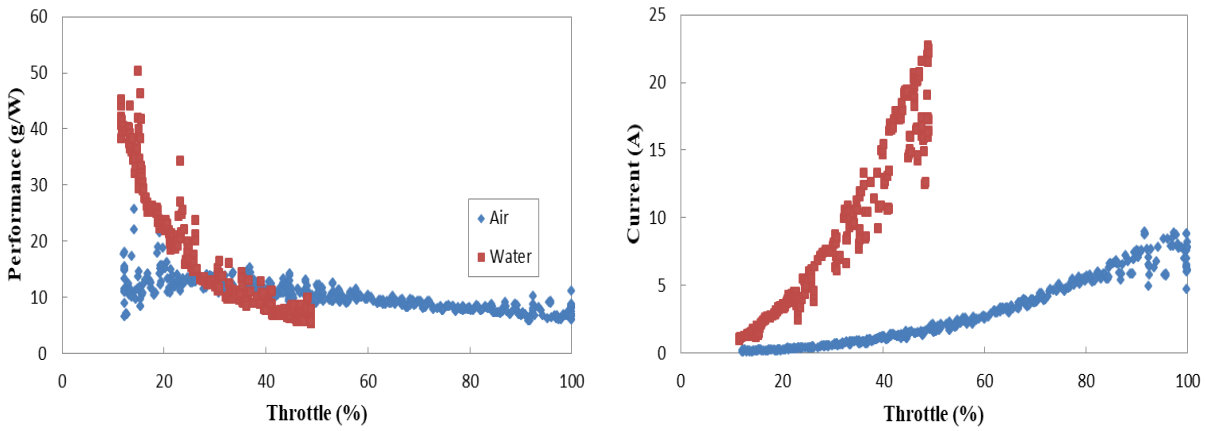

Figure 25. Performance of the T-motor 13 by 4.4 inch carbon fiber propeller in air and water. Underwater data was concluded at 40% throttle due to high current consumption.

Next, the performance for the T-motor MN4006-23 motor with the 13 inch propeller was examined. Similar to the small propeller, at low throttle levels, the performance underwater is observed to be greater than air, but for this motor-propeller combination, the underwater performance is observed to be less than in air (Figure 25). This is a result of the motor being designed for low torque operations. At higher torques, the motor requires more power to operate, but will be unable to produce the proper amount of thrust to be efficient. Underwater testing was concluded due to high currents approaching the current sensor limit.

Testing on the U10 motor with the 28 inch propeller continued without the torque sensor, as the data collected was insufficient to properly observe the performance underwater. It is observed in Figure 26 that the performance of this combination mirrors the smallest combination rather than the medium sized combination. Like the small motor, the performance underwater for the large combination begins at high values, but then proceeds to gradually decrease. Similar to the previous case, the underwater testing for the largest motor-propeller combination was concluded to high currents approaching the current sensor limit.

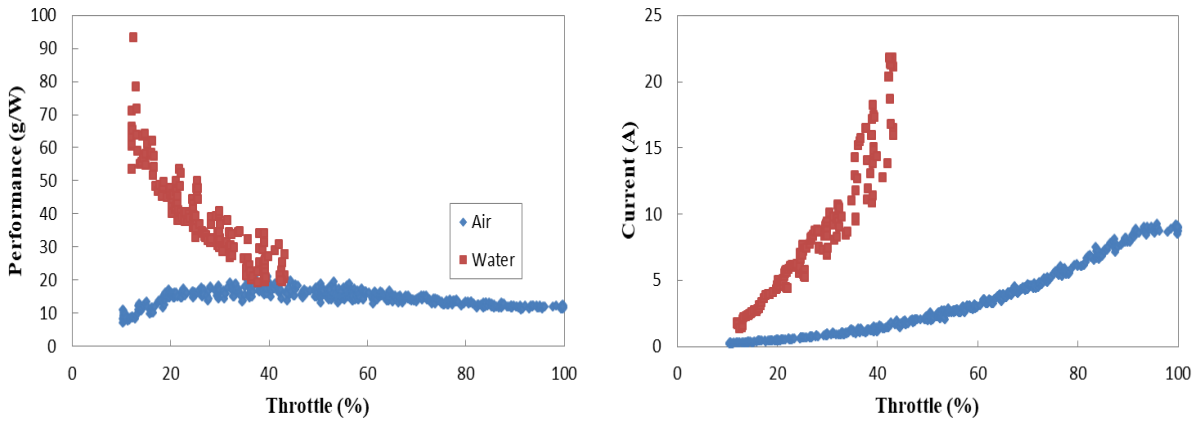

Figure 26. Performance of the T-motor 28 by 9.2 inch carbon fiber propeller in air and water. Underwater data was concluded at 40% throttle due to high current consumption.

When comparing the performances of the three combinations in air, motor-propeller combinations are observed to perform better as the size is increased. From Figure 27, it is observed that as motor-propeller size increases, so does changes in range of performance. Compared to the medium and large sized combinations, the small combination has a consistent performance throughout the throttle range. The medium and large sized combinations are observed to drop in performance as throttle is increased, but still remains greater than the previous motor-propeller size.

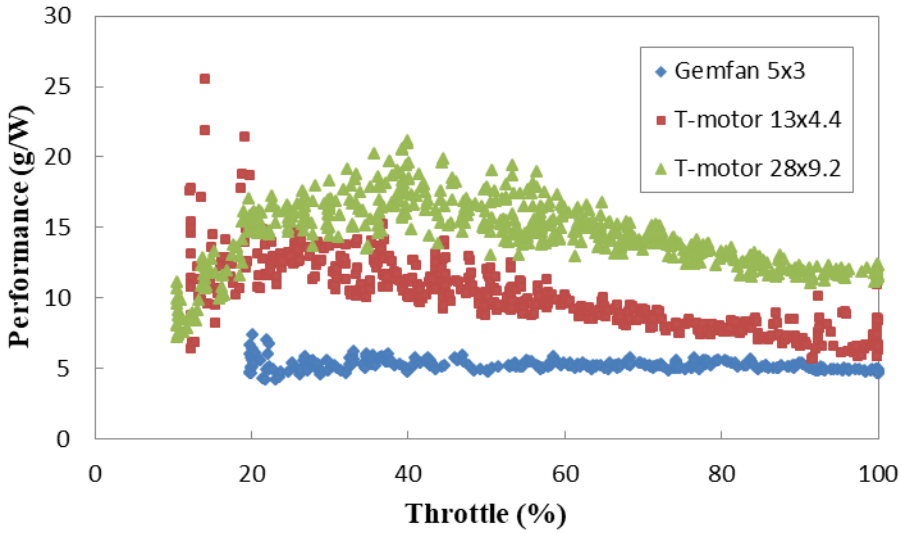

Figure 27. Comparison of the performances of the three motor-propeller combinations in air.

The largest motor-propeller combination remains as the superior option for underwater performance, as shown in Figure 28. Despite having the lowest performances of the three combinations observed in air, it is observed that the small sized combination performs better than the medium sized combination underwater. Although it was shown that the medium sized motor-propeller combination will produce more thrust than the small combination, the medium combination is less efficient underwater.

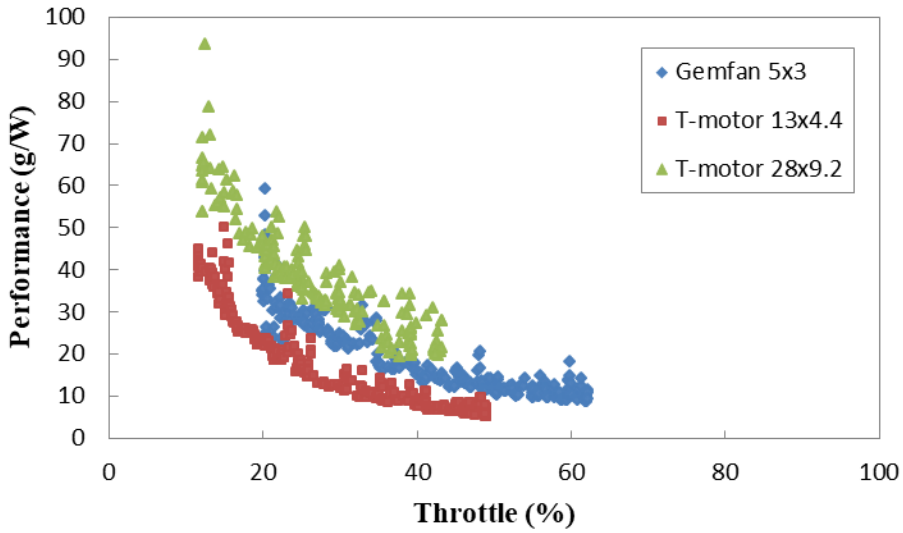

Figure 28. Comparison of the performances of the three motor-propeller combinations underwater.

The medium sized motor was then examined just as the large motors were in the previous section. Motor curves for the T-motor MN4006-23 motor were created to determine whether the motor is responsible for the inconsistency observed in underwater performance in Figure 29.

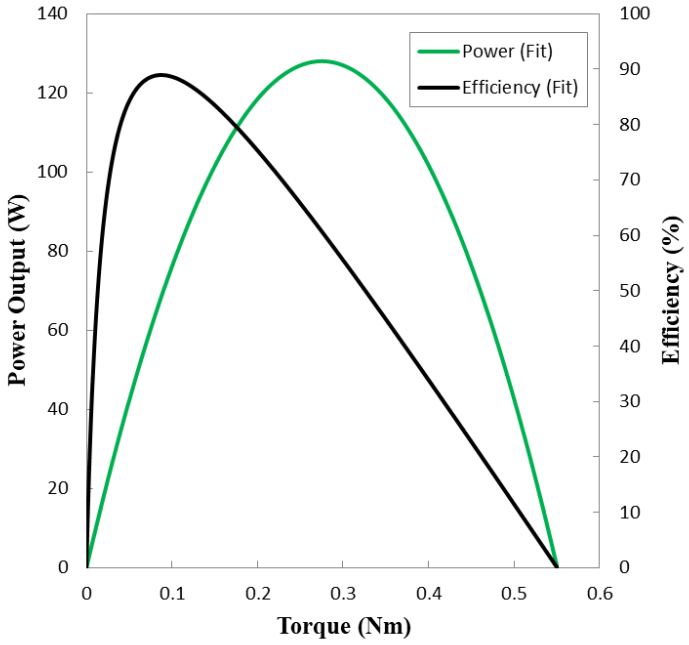

Figure 29. Power and efficiency curves for the T-motor MN4006-23 motor.

Figure 29 shows the results of the motor curve for the medium sized motor. It is observed that this motor is a low torque motor, which is very efficient in air due to the small range of torque between the peak of the efficiency curve and the power output curve. Despite the efficiency in air, as shown in all water tests, a great amount of torque is introduced to the system when run underwater. As a result, the low stall torque of this motor can be attributed as the reason for the low performance of this motor underwater.

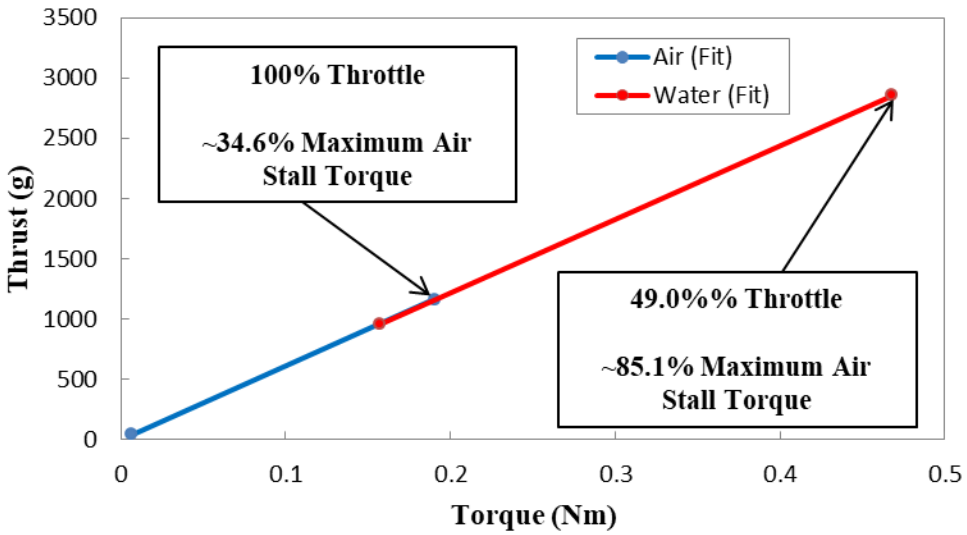

Figure 30. Maximum torque comparison for the medium motor-propeller combination. In air, the maximum torque produced was only 34.6% of the stall torque for the T-motor MN4006-23 motor. Underwater it was 85.1%.

Figure 30 reshows the torque-thrust linear relation for the 13 inch propeller. Having the results from the motor curves from Figure 29, the amount of torque produced in air and water can be better observed with respects to the maximum air stall torque of the medium sized motor. In air, the maximum torque for this motor combination was observed at maximum throttle with 34.6% of the maximum stall torque, whereas underwater it was at 49.0% throttle where the combination produced 85.1% of the maximum air stall torque. For reference, the small combination produced 5.3% of its maximum stall torque in air and 58.1% underwater; the large combination produced 13.3% in air and 61.8% underwater.

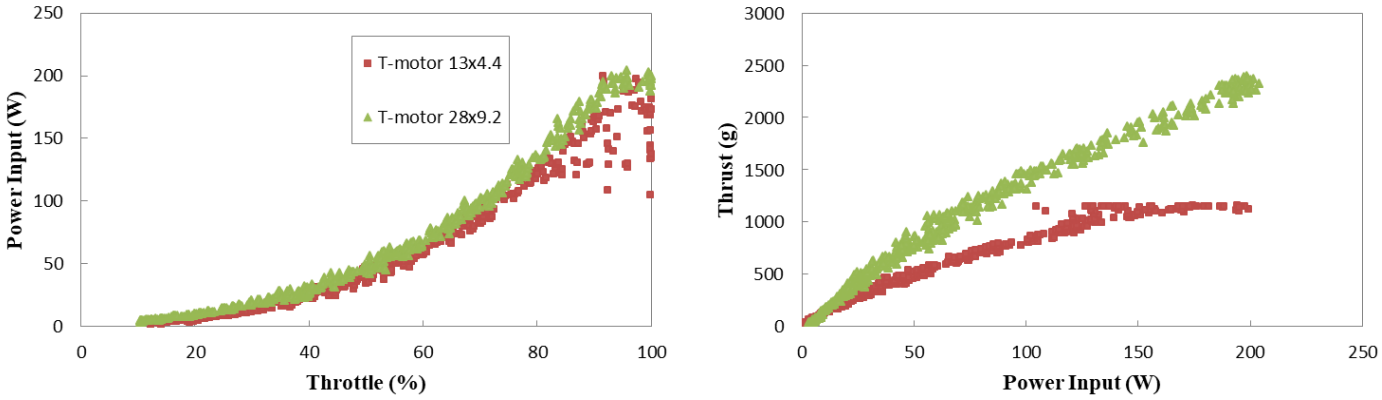

Figure 31. Power input comparison for the medium and large sized motor-propeller combination in air.

Further analysis on the medium and large motor-propeller combinations was done to examine the effect of scaling up the size of the propulsion system of the current UAV-UUV, the Naviator. Figure 31 shows that at the same throttle, the same amount of power is supplied to the motors for the same input voltage. As was shown in the performance, the larger of the two motor-propeller combination produces much more thrust per power input. This trend is also observed underwater as shown in Figure 32.

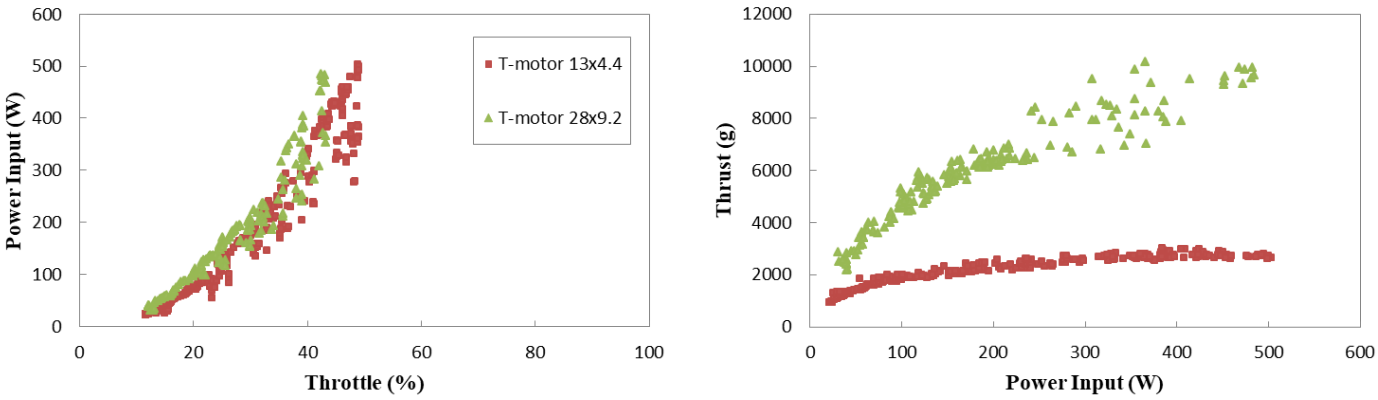

Figure 32. Power input comparison for the medium and large sized motor-propeller combination underwater.

4. Conclusion

The objective of this study was to observe the effects of scaling on an aerial-underwater vehicle. Motor tests were conducted to explore how different sizes of motors perform under varying torque loads. Propellers were then equipped to these motors and evaluated in air and underwater.

Motor curves were generated using the two of the largest commercially off-the-shelf motors, the T-motor U8 Pro and T-motor U10 motors. At the same voltage power input of 22.2V, it was found that the T-motor U10 motor is capable of a much larger mechanical power output and torque load (with a higher stall torque). Due to the higher torque load, the U10 motor was also more efficient under heavier loads. These two motors were then compared to the other two motors examined in this study, the NTM Propdrive 28-26 motor and the T-motor MN4006-23 motors, in order to observe the effect of the increase in motor size. From this section of the

study, it was determined that the T-motor U10 motor would be used as the large-sized motor for the motor-propeller section.

Three motor-propeller combinations, each with a carbon fiber propeller, were examined: the NTM Propdrive 28-26 motor with a Gemfan 5 by 3 inch propeller, the T-motor MN4006-23 motor with a T-motor 13 by 4.4 inch propeller, and the T-motor U10 motor with a T-motor 28 by 9.2 inch propeller. Torque and thrust for each combination was observed to maintain a linear relation regardless if in air or in water. When increasing the size of motors and propellers, the range of torque and thrust generated increases, but the linear ratio decreases.

Performance on each motor combination in air showed that increasing the size also increased the performance of the system. Underwater, it is observed that performance tends to be greater than in air. However, as throttle increased, the underwater performance would drastically decrease; so much so that the medium sized combination was found to perform worse than in air. In addition, it was observed that this combination performed the worst of the three underwater.

Testing on the T-motor MN4006-23 motor was done to determine the cause of the inconsistency observed between air and water results. It was found that this motor had a low stall torque. The maximum torque detected for this motor underwater was 85.1% of the maximum air stall torque.

4.1. Future Experiments

As with all experimentation, repetition of all the experiment conducted in this study would be required to further verify the results. In addition, more motor and propeller combinations could be considered for future use. This could assist in future decisions for selecting the most optimal motor-propeller combination for a multi-medium vehicle.

Motor tests were only conducted in air for this study. As such the effect of water on the motor curves has yet to be explored, and could further assist in understanding inconsistencies that may occur in the future.

In addition, it would be valuable to equip test vehicles with larger motors and propellers to observe practical applications of this study. For instance, the testing vehicle can be used to carry payloads in air and underwater with the increase of thrust generated from the larger system.

5. References

1. Qiang Wang. “The Current Research Status and Prospect of Multi-Rotor UAV.” IOSR Journal of Mechanical and Civil Engineering (IOSR-JMCE) , vol. 14, no. 4, 2017, pp. 31–35.
2. H. Otsuka and K. Nagatani, "Thrust loss saving design of overlapping rotor arrangement on small multirotor unmanned aerial vehicles," *2016 IEEE International Conference on Robotics and Automation (ICRA)*, Stockholm, 2016, pp. 3242-3248.
3. Muchiri, N., and S. Kimathi. "A Review of Applications and Potential Applications of UAV." *Proceedings of Sustainable Research and Innovation Conference*. 2016.
4. Pandit, DAP Dr Vinay, and Arun Poojari. "A study on amazon prime air for feasibility and profitability--a graphical data analysis." *IOSR Journal of Business and Management* 16.11 (2014): 06-11.
5. Maia, Marco M., Parth Soni, and Francisco J. Diez. "Demonstration of an aerial and submersible vehicle capable of flight and underwater navigation with seamless air-water transition." *arXiv preprint arXiv:1507.01932* (2015).
6. Bershadsky, Dmitry, Stephen Haviland, and Eric N. Johnson. "Electric Multirotor Propulsion System Sizing for Performance Prediction and Design Optimization." *AIAA SciTech* (2016).
7. Winslow, Justin, et al. "Design, development, and flight testing of a high endurance micro quadrotor helicopter." *International Journal of Micro Air Vehicles* 8.3 (2016): 155-169.
8. Merchant, Monal P., and L. Scott Miller. "Propeller performance measurement for low Reynolds number UAV applications." *AIAA* 1127 (2006): 2006.

9. Brandt, John B., and Michael S. Selig. "Propeller performance data at low reynolds numbers." *49th AIAA aerospace sciences meeting*. 2011.
10. Yoon, Seokkwan, Henry C. Lee, and Thomas H. Pulliam. "Computational Analysis of Multi-Rotor Flows." (2016).
11. Intaratep, Nanyaporn, et al. "Experimental study of quadcopter acoustics and performance at static thrust conditions." *22nd AIAA/CEAS Aeroacoustics Conference*. 2016.
12. Aleksandrov, D., and I. Penkov. "Optimal gap distance between rotors of mini quadrotor helicopter." *Proceedings of the 8th DAAAM Baltic Conference, Tallinn, Estonia*. 2012.
13. Ryll, Markus, Heinrich H. Bülthoff, and Paolo Robuffo Giordano. "First flight tests for a quadrotor UAV with tilting propellers." *Robotics and Automation (ICRA), 2013 IEEE International Conference on*. IEEE, 2013.
14. Soni, P. V., "Characterization and Optimization of UAV Power System for Aerial and Submersible Multi-Medium Multirotor Vehicle," Master's Thesis, School of Engineering, Rutgers Univ., New Brunswick, NJ, 2016.
15. Yedamale, Padmaraja. "Brushless DC (BLDC) motor fundamentals." *Microchip Technology Inc* 20 (2003): 3-15.
16. Shao, Jianwen, Dennis Nolan, and Thomas Hopkins. "A novel direct back EMF detection for sensorless brushless DC (BLDC) motor drives." *Applied Power Electronics Conference and Exposition, 2002. APEC 2002. Seventeenth Annual IEEE*. Vol. 1. IEEE, 2002.
17. Pillay, Pragasen, and Ramu Krishnan. "Modeling, simulation, and analysis of permanent-magnet motor drives. II. The brushless DC motor drive." *IEEE transactions on Industry applications* 25.2 (1989): 274-279.

18. Theys, Bart, et al. "Influence of propeller configuration on propulsion system efficiency of multi-rotor Unmanned Aerial Vehicles." *Unmanned Aircraft Systems (ICUAS), 2016 International Conference on*. IEEE, 2016.